JOURNAL OF GEOPHYSICAL RESEARCH, VOL. 102, NO. D16, PAGES 19,559–19,573, AUGUST 27, 1997

Subgrid-scale rainfall variability and its effects on atmospheric and surface variable predictions

Shuxia Zhang and Efi Foufoula-Georgiou

St. Anthony Falls Laboratory, University of Minnesota, Minneapolis

Abstract. A new approach, which combines the Penn State/National Center for Atmospheric Research mesoscale model MM5 with a recently developed statistical downscaling scheme, has been investigated for the prediction of rainfall over scales (grid sizes) ranging from the atmospheric model scale (> 10 km) to subgrid scale (around 1 km). The innovation of the proposed dynamical/statistical hybrid approach lies on having unraveled a link between larger-scale dynamics of the atmosphere and smaller-scale statistics of the rainfall fields [*Perica and Foufoula-Georgiou*, 1996a], which then permits the coupling of a mesoscale dynamical model with a small-scale statistical parameterization of rainfall. This coupling is two-way interactive and offers the capability of investigating the feedback effects of subgrid-scale rainfall spatial variability on the further development of a rainfall system and on the surface energy balance and water partitioning over the MM5 model grids. The results of simulating rainfall in a strong convection system observed during the Oklahoma-Kansas Preliminary Regional Experiment for STORM-Central (PRESTORM) on June 10-11, 1985 show that (1) the dynamical/statistical hybrid approach is a useful and cost-effective scheme to predict rainfall at subgrid scales (around 1 km) based on larger-scale atmospheric model predictions, and (2) the inclusion of the subgrid-scale rainfall spatial variability can significantly affect the surface temperature distribution and the short-term (< 24 hour) prediction of rainfall intensity.

1. Introduction

Atmospheric dynamics are described by a set of partial differential equations expressing the conservation of mass, energy and momentum in the atmosphere. The solution of these equations at a discretized mesh covering the domain of interest is the basis of numerical weather prediction models. It is understood that solving these equations over a very fine mesh (grid size of the order of a few kilometers) covering a large area is computationally prohibitive, especially for lengthy simulations or ensemble predictions. Moreover, even if the power of future computers makes very high resolution atmospheric modeling possible, it is still uncertain that this would significantly improve the accuracy of prediction of atmospheric variables (at least with the microphysical parameterizations currently used in many mesoscale models). Besides, there might be inherent limitations in very fine scale atmospheric predictions. For example, it has been recently suggested that the unstable and chaotic character of the atmosphere renders prediction of fine-scale variables less accurate than prediction of larger-scale variables, simply because space-time averaging reduces the degree of variability of the atmospheric system and the "effective dimensionality" of the underlying attractor [e.g., *Vannitsem and Nicolis*, 1994, 1995]. Thus, it might be that apart from computational difficulties, there are inherent limitations in physically predicting atmospheric variables, such as rainfall, at very fine scales. Therefore, the need arises to investigate in parallel other statistically based methods for resolving rainfall variability at very fine scales.

Recently, *Perica and Foufoula-Georgiou* [1996b] introduced a new spatial rainfall downscaling scheme which, conditional on large-scale rainfall averages and thermodynamic properties of the prestorm environment, successfully reconstructs smaller-scale rainfall variability. The premise of this downscaling scheme is based on two main findings of *Perica and Foufoula-Georgiou* [1996a], which were extensively documented for several midlatitude mesoscale convective systems. These are that (1) standardized rainfall fluctuations exhibit normality and simple scaling over the mesoscale (e.g., from 4x4 km^2 to 64x64 km^2), and (2) the statistical scaling parameterization of these standardized rainfall fluctuations (which in essence reflects the way rainfall energy is distributed across scales) relates to the convective instability of the prestorm environment as measured, for

Paper number 97JD01392.
0148-0227/97/97JD-01392$09.00

example, by CAPE (convective available potential energy).

The work reported in this paper aims at (1) the development of a hybrid approach that couples the statistical downscaling scheme of *Perica and Foufoula-Georgiou* [1996b] with the Penn State/National Center for Atmospheric Research mesoscale model MM5 for the purpose of predicting rainfall over a wide range of scales, from a few kilometers to several hundred kilometers in horizontal extent, and (2) the use of this hybrid model to study the effect of subgrid-scale rainfall variability on short-term rainfall and ground temperature prediction. The innovation of the proposed dynamical/statistical hybrid approach lies in taking advantage of the link between larger-scale dynamics of the atmosphere and smaller-scale statistics of the rainfall fields [*Perica and Foufoula-Georgiou*, 1996a], which then permits the coupling of a mesoscale dynamical model, such as the MM5, with a small-scale statistical parameterization of rainfall.

The newly developed hybrid approach is verified by a control run of simulating rainfall development in a strong convection system as observed on June 10-11, 1985 in the Preliminary Regional Experiment for STORM-Central (PRESTORM). This case was selected because it falls within the midlatitude mesoscale convective systems studied by *Perica and Foufoula-Georgiou* [1996a], and thus the predictive relationships between meteorological and statistical descriptors of storms, forming the basis of the spatial downscaling scheme, are known to hold for this storm. Also, several studies [e.g., *Zhang et al.*, 1989] have provided detailed examination of the dynamical features of this storm and its prediction using an atmospheric model, and thus provide useful information for our study. Our results indicate that the dynamical/statistical hybrid approach is a useful and cost-effective scheme to predict rainfall at subgrid scales (around 1 km) based on larger-scale atmospheric model predictions. They also show that improved short-term (< 24 hour) rainfall predictions at various scales can be obtained by considering the subgrid-scale land-atmosphere interactions via a two-way interactive coupling of the atmospheric model with the proposed rainfall downscaling scheme. These findings demonstrate that better understanding of the small-scale spatio-temporal rainfall variability promises not only better prediction of hydrologic variables such as basin runoff, but also better prediction of rainfall itself through coupled modeling.

2. Model Description

2.1. Statistical Downscaling Scheme

Based on the statistical analysis of several storms from the PRESTORM field program in May and June 1985 (see *Cunning* [1986] for details on that program), *Perica and Foufoula-Georgiou* [1996a] found that "standardized rainfall fluctuations" exhibit normality and simple scaling (self-similarity). Standardized rainfall fluctuations, $\xi_{L,j}$ at scale L and direction j ($j = 1, 2, 3$ respectively representing the longitude, latitude and diagonal directions), were defined as

$$\xi_{L,j} = \frac{X'_{L,j}}{\overline{X}_L} \tag{1}$$

where $X'_{L,j}$ is the rainfall intensity gradient at scale L and direction j (obtained via a multiscale directional filtering of spatial rainfall intensities with Haar wavelet) and $\overline{X}_L$ is the average rainfall intensity at the same scale L (obtained via filtering with the "scaling function" complementary to the chosen wavelet). Mathematical details of this wavelet decomposition can be also found in the work by *Kumar and Foufoula-Georgiou* [1993a,b]. The simple scaling of $\xi_{L,j}$ implies that

$$\frac{\sigma_{\xi,L_1\times L_1}}{\sigma_{\zeta,L_2\times L_2}} = \left(\frac{L_1}{L_2}\right)^H \tag{2}$$

where $\sigma_{\xi,L_1\times L_1}$ denotes the standard deviation of ξ at scale L_1 (kilometers) and H is a scale invariant exponent. They also found that despite the strong directionality of rainfall intensities in several squall line storms observed during the PRESTORM experiment, the standardized rainfall fluctuations were almost isotropic and the value of H (which varied between 0.1 and 0.35 for different storms) was not significantly dependent on direction. Thus, the average value of H over the three directions was used to represent the scaling of the standardized rainfall fluctuations.

In the work by *Perica and Foufoula-Georgiou* [1996a], the self-similarity of standardized rainfall fluctuations was documented for scales between 4×4 km^2 and 64×64 km^2. The lower scale of 4 km was imposed by the radar data resolution and the upper scale of 64 km was selected so that enough averaging cells within the radar images were available for a meaningful statistical analysis. The analyzed scales were selected dyadically for computational efficiency in implementation of the discrete Haar wavelet transform.

It is noted from (2) that if one knows the value of σ_ξ at one particular reference scale and the value of H, the σ_ξ at any other scale can be easily computed. In the work by *Perica and Foufoula-Georgiou* [1996a], that reference scale was chosen to be the 8 km scale as this was the smallest scale at which wavelet fluctuations were defined. (Note that the smallest scale at which fluctuations via a wavelet transform are defined is one dyadic scale larger than the observation scale, which was 4 km).

Perica and Foufoula-Georgiou [1996a] demonstrated that for midlatitude mesoscale convective systems, H and $\sigma_{\xi,8\times8}$ are related to the convective available potential energy ($CAPE$) ahead of the storm (a measure of the convective instability of the prestorm environment) by the following empirical relationships:

$$H = 0.052 + 0.965\ CAPE \times 10^{-4},\ R = 0.82 \quad (3)$$

$$\sigma_{\xi,8\times8} = 0.539 - 0.853\ CAPE \times 10^{-4},\ R = -0.73 \quad (4)$$

where $CAPE$ is in square meters per second squared, H and $\sigma_{\xi,8\times8}$ are dimensionless, and R denotes the coefficient of the linear regression. Equations (3) and (4) led for the first time to establishing relationships between statistical scaling and thermodynamic parameters of storms.

Based on these relationships a new physical/statistical scheme for multiscale rainfall disaggregation (downscaling) was developed by *Perica and Foufoula-Georgiou* [1996b]. This scheme uses an inverse wavelet transform (IWT) to obtain rainfall intensities at any scale smaller than the initial scale (e.g., from 64×64 km^2 averages down to 4×4 km^2 averages in that study). In the present study, it is assumed that the simple scaling regime extends to scales below 4×4 km^2 and in particular that it applies down to scales of 1.5×1.5 km^2. A further description of the implementation of the downscaling scheme is presented in section 2.3.

2.2. The Atmospheric Model MM5

The Penn State/NCAR Mesoscale Model MM5 is one of the most widely used state-of-the-art atmospheric modeling systems. It solves the full set of dynamical equations that describe the conservation of mass, momentum and energy in the atmosphere and a set of microphysics equations for different phase clouds and precipitation. It has multiple-nest capability, hydrostatic or nonhydrostatic dynamics, and four-dimensional data assimilation capability, as well as many physics options [*Grell et al.*, 1994].

The MM5 is used in this study to compute rainfall over the model grids and the dynamical features associated with the storm environment. Because the statistical downscaling equations are based on the analysis of radar rainfall intensity fields (which are considered as instantaneous rainfall intensities representative of a 7 to 10 min interval), we have modified the MM5 code to give a similar rainfall product as output (instead of rainfall accumulation). Specifically, using a simulation time step of 1.0 min, we have approximated instantaneous rainfall intensities by the average of computed rainfall accumulations over 10 time steps divided by the averaging time of 10 min. This averaging can also help to avoid numerical instabilities in rainfall computation and provides a smoothing of the highly variable 1 min rainfall predictions to a more meaningful product.

2.3. Coupling the Statistical Downscaling Scheme With the MM5

As seen in (3) and (4), $CAPE$ is the key parameter linking the statistical scaling description of rainfall with the atmospheric dynamics of the storm. Physically, $CAPE$ measures the convective instability of a parcel of air at a given location in a storm environment. Quantitatively, $CAPE$ is evaluated either from sounding data at the observation stations or from variables predicted with an atmospheric model at all grid points of the model [*Air Weather Service*, 1979]. Since there are several ways to compute $CAPE$ in meteorological applications and dramatically different values can be obtained for the same sounding data depending on the height from which a parcel of air is assumed to rise, and also on the thermal or mechanical causes of the rising [*Air Weather Service*, 1979], we present here a detailed description of the procedure that we have followed in our computation.

In this study, $CAPE$ is considered as a dynamical two-dimensional variable, which varies both temporally and spatially. At a given time instant, the value of $CAPE$ at any grid point i inside the studied region is defined as

$$CAPE = A \int_{LFC}^{EL} (T_{sa} - T) d\tilde{p} \quad (5)$$

where LFC is the level of free convection, EL is the equilibrium level, T is temperature, $\tilde{p} = (P/P_o)^{0.286}$ with P being pressure and P_o reference pressure (1000 millibars), $A = -4186.8$ m^{2}s^{-2}K^{-1} is unit converting factor (the negativeness of A is due to the fact that the pressure at LFC is greater than that at EL) and T_{sa} is the saturated adiabat crossing the lifted condensation level (LCL), to which a parcel of air from the lowest 500 m of the atmosphere rises dry adiabatically until saturated and wet adiabatically thereafter. T, $\tilde{p}$, and T_{sa} are determined at the grid point i as functions of vertical levels (or height) [*Air Weather Service*, 1979].

The temperature (degrees Kelvin) and pressure (millibars) at the LCL are given by

$$T_{LCL} = 56 + \frac{1}{(T_{dew} - 56) + \log(T_{500}/T_{dew})\, 800} \quad (6)$$

$$P_{LCL} = P_{500}\, (T_{LCL}/T_{500})^{3.5} \quad (7)$$

where T_{500}, T_{dew} and P_{500} are respectively the temperature, dew point and pressure at the height of 500 m above the ith grid point on the ground. Equations (6) and (7) are adopted from the general meteorological package (GEMPAK) [*University Corporation for Atmospheric Research*, 1992] to be consistent with the evaluation of $CAPE$ used by *Perica and Foufoula-Georgiou* [1996a] in developing the predictive relationships (3) and (4).

The statistical downscaling scheme uses $CAPE$ not as a single point value but rather as a storm representative parameter describing the potential for convective instability in the environment ahead of the storm development. Thus instead of using point values of $CAPE$, we have introduced a representative value denoted by $< CAPE >$ and defined as

$$< CAPE >= \frac{1}{N_s} \sum_{i=1}^{N_s} CAPE_i \cdot I_{K_s,i} \qquad (8)$$

where $CAPE_i$ is the convective available potential energy determined using (5) at each grid point i inside the studied region, N_s is the number of grids at which $CAPE_i$ is greater than a selected value K_s, and $I_{K_s,i}$ is an indicator function being either 0 or 1 depending on whether $CAPE_i$ is lower or greater than K_s, i.e., $I_{K_s,i} = 0$ if $CAPE_i < K_s$ or $I_{K_s,i} = 1$ if $CAPE_i > K_s$. Introduction of (8) for the representative $< CAPE >$ is not arbitrary, but is based on the character of the spatial distribution of the convective energy and its change during the storm evolution. Further discussion on this point and on selecting the appropriate value of K_s is presented in section 3.2.

Equations (3) and (4) form the basis for developing an interactive dynamical coupling of the statistical downscaling scheme with the MM5. By interactive coupling we mean that we not only predict the subgrid scale rainfall variability at every time step of the atmospheric simulation, but its feedback effects are also taken into account in predicting the further development of rainfall, surface energy balance and water partitioning over the MM5 model grids. This two-way interactive coupling is carried out by adding two new modules to the MM5 code. One module is named SDS (statistical downscaling scheme). The other is named FERSV (feedback effects of rainfall spatial variability). These two modules are called once every 10 time steps (recall our time step is 1 min) after the instantaneous rainfall is computed by the MM5 model. One can call SDS alone if the interest is to predict only the small-scale rainfall variability without worrying about the spatial redistribution of moisture and heat fluxes and their effects on the surface water and energy partitioning.

The SDS first computes $CAPE$ (equation (5)) at each grid i on the ground at a given time instant and determines a representative $< CAPE >$ (equation (8)) for the studied region. Then the SDS redistributes the rainfall from the MM5 grid mesh onto the subgrid mesh by using the statistical downscaling scheme according to the determined value of $< CAPE >$. Briefly, the downscaling scheme is implemented as follows: once $< CAPE >$ is known, H and $\sigma_{\xi,8\times8}$ are computed from (3) and (4). Then, standardized rainfall fluctuations at any other scale $L \times L$ km^2 are generated from a Gaussian distribution with zero mean and standard deviation $\sigma_{\xi,L\times L}$, which is related to $\sigma_{\xi,8\times8}$ by

$$\sigma_{\xi,L\times L} = \sigma_{\xi,8\times8} \left(\frac{L}{8}\right)^H \qquad (9)$$

These fluctuations are then randomly distributed in space over grid boxes at scale $L \times L$ km^2 and are multiplied by the corresponding local rainfall average values at that same scale. Then they are "added" via an inverse wavelet transform (IWT), to these averages to get rainfall intensities at the next finer scale. This procedure is repeated at all intermediate scales down to the finest scale of interest (see *Perica and Foufoula-Georgiou* [1996b] for more details and for an implementation algorithm). The subgrid mesh grid length is made 1/2, 1/4, 1/8 ... times smaller than the original MM5 grid length, until the smallest scale of interest. Note that because the Haar wavelet transform is a reconstructive filter, the average rainfall intensities are not only preserved over the whole domain of interest, but are also preserved locally inside each MM5 grid box and at all subgrid scales within it.

The feedback effects of subgrid-scale rainfall variability are computed in the FERSV module by evaluating the changes of ground temperature, heat and moisture fluxes in the subgrid regime under the assumption that moisture availability M not only is laterally heterogeneous, but also varies in time as a function of local rainfall intensity. In order to be self-consistent, roughness Z_L and thermal capacity C_{ap}, which are the other physical parameters essential for solving the energy and water budget equations, are adjusted correspondingly. The dependence of M, Z_L and C_{ap} on the local rainfall intensity is described in the appendix. The Blackadar high-resolution boundary layer model [*Grell et al.*, 1994] has been modified so that the energy and water balances at the ground are determined in the subgrid regime, taking into account the changes of M, Z_L and C_{ap} associated with the subgrid-scale rainfall intensity. Then the ground temperature, heat and moisture fluxes evaluated in the subgrid regime are extrapolated onto the MM5 model grids. This adjustment provides the bottom boundary conditions for the MM5 model to compute the dynamical features of next time step, thus resulting in the interactive coupling of the statistical downscaling scheme with the dynamical model.

2.4. Advantages of the Hybrid Approach

The statistical/dynamical hybrid approach presented in this paper for rainfall downscaling offers great advantages over many currently used approaches. First, it is dynamical in the sense that the parameters of the subgrid-scale scheme are updated as the storm evolves based on the evolution of the convective instability of the storm environment as measured by the $CAPE$. Second, its parameterization is scale-independent and thus offers the capability of resolving the subgrid-scale rainfall variability at any selected scale without the need to consider a separate parameterization at each scale (at least within the studied scales of 4x4 to 64x64 km^2). Third, as was demonstrated by *Perica and Foufoula-Georgiou* [1996b], the proposed downscaling scheme has the ability to accurately reconstruct the percent of area covered by storm at all subgrid scales.

All these advantages are missing from current simple rainfall subgrid scale parameterization schemes (see *Thomas and Henderson-Sellers* [1991] for a review). For

example, a very common scheme [e.g., *Schaake et al.*, 1996; *Warrilow et al.*, 1986] consists of specifying the fraction of area covered by rain at the scale of interest, e.g., 30%, and an exponential distribution with fixed parameters for redistribution of rainfall at the desired scale. This scheme typically does not have the ability to dynamically update its parameters (i.e., the fraction of area covered by storm and the parameter of the exponential distribution) as the storm evolves, nor does it have the ability to consider the scale dependence of these parameters.

It is known, however, that both the fraction of area covered by the storm and the parameter of the statistical distribution of rainfall intensities strongly depend on scale. For instance, *Kumar and Foufoula-Georgiou* [1994] and *Perica and Foufoula-Georgiou* [1996b] reported that for midlatitude mesoscale convective systems the fraction of the area covered by the storm changes from $20-30\%$ at a scale of 4×4 km^2 to $60-70\%$ at a scale of 64×64 km^2. These percentages and their dependence on scale depend on the storm type and may change dramatically as the storm evolves from the buildup to dissipation stages [e.g., *Seo and Smith*, 1996; *Fan et al.*, 1996]. Our scheme allows for a dynamical updating of these parameters during the storm evolution based on the variation of $< CAPE >$ computed with the atmospheric model.

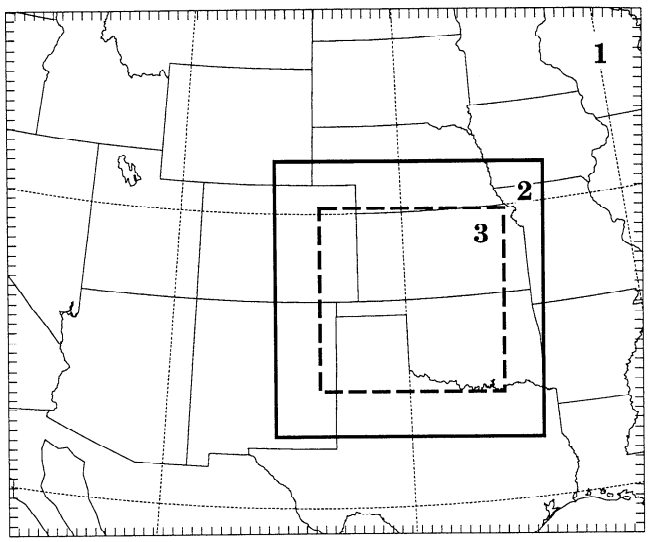

Figure 1. Model domain consisting of three nested domains, named domain 1, domain 2, and domain 3 with resolutions of 36 km (outer frame), 12 km (inner solid frame), and 4 km (dashed frame), respectively.

3. Model Verification and Results

3.1. Modeled Storm

In order to show the capability of the newly developed hybrid approach to model rainfall variability at a range of scales, we will report in this section the results of simulating the rainfall development of the June 10-11, 1985 PRESTORM squall line system. The dynamical model consists of three nested domains (named respectively domain 1, domain 2 and domain 3 in Figure 1) in the horizontal direction and 23 levels of vertical terrain-following coordinate σ. The grid size of domain 1 (the outside frame in Figure 1) is 36 km, of domain 2 (the inner solid frame) is 12 km, and of domain 3 (the inner dashed frame) is 4 km. The numbers of three dimensional grid boxes in the domains 1, 2, and 3 are $55 \times 67 \times 23$, $85 \times 85 \times 23$, and $163 \times 163 \times 23$, respectively. The dynamical model is initiated at 1200 UTC June 10, 1985 using the conventional preprocessing procedures (see *Zhang et al.* [1989] for a detailed description). Several sets of various physics options available in the MM5 code combined with different model resolutions have been tested with the purpose of producing rainfall fields that resemble the observed ones as closely as possible. The simulation results will be reported for four runs, whose variable resolution is achieved by using the multinesting capability of the MM5 model [*Grell et al.*, 1994]. The domain of these runs and their nesting structure (summarized in Table 1) will be described below in combination with presenting the simulation results obtained with each run. Table 2 lists the physics options used for each of the three nested domains when that domain is turned on. All the results will be shown for the area covered by domain 2, but with different resolutions corresponding to different runs listed in Table 1.

Among all the performed tests, the best fit between simulated and observed rain for the June 10-11, 1985 storm has been obtained with run 1 using the specified physics options for domains 1 and 2 as listed in Table 2. The goodness of fit is measured here in terms of capturing the correct timing and location of the storm system as compared to the observations. In run 1, domain 3 is

Table 1. Summary of the MM5 Simulation Runs for Which the Results Are Reported in This Paper

Simulations	Domain 1 (36 km Resolution)	Domain 2 (12 km Resolution)	Domain 3 (4 km Resolution)	Subgrid-regime* (1.5 km Resolution)
Run 1	on	on	off	off
Run 2	on	on	off	on
Run 3	on	off	off	off
Run 4	on	on	on	off

* Subgrid-regime is implemented in Domain 2

Table 2. Physics Options Used for Each Nested Domain Shown in Figure 1

Parameter	Domain 1	Domain 2	Domain 3	Physical Meaning
NHYDRO	1	1	1	nonhydrostatic run
FRAD	3	3	3	CCM2 radiation scheme
FUPR	1	1	1	upper radiative BC
MPHYS	4	6	6	simple ice and Graopel-GSFC
BOUDY	3	2	2	boundary conditions
BLTYP	2	2	2	Blackadar PBL
DRY	0	0	0	moist convection
MOIST	2	2	2	rain prediction
ICUPA	3	5	1	Grell, FC and none cumulus scheme
SFFLX	1	1	1	with surface fluxes
TGFLG	1	1	1	with ground temperature
SFPAR	1	1	1	13 land use categories
CLOUD	1	1	1	cloud effect on radiation

BC denotes boundary condition, GSFC denotes Goddard Space Flight Center, PBL denotes planetary boundary layer, Grell and FC denote Grell and Fritsch/Chappell cumulus parameterization schemes.

turned off while domain 1 and domain 2 are kept two-way interactive. The results (e.g., Figure 2) obtained with this run are hence taken as the reference point in this study for assessing the feedback effect of subgrid-scale rainfall variability (run 2 versus run 1) and the effects of changing the MM5 model resolutions (run 3 and run 4 vs run 1).

Before the results are presented, some clarifications are in order. In the MM5 model, the computation of rainfall consists of two components. One is called "resolved rainfall" and is determined by explicitly solving the cloud and rainwater equations over the MM5 model grids. The other part is called "convective rainfall" and is determined by the parameterization scheme of convective cumulus. The concept of resolved and convective rainfall partition was developed for large-scale atmospheric models with grid length greater than several tens of kilometers. The resolved rainfall component so computed was assumed to correspond to rainfall formed by the lifting of moist air up to a condensation level in stable stratification and to be related to large-scale synoptic systems. The convective rainfall component was assumed to correspond to rainfall generated by convective systems with strong lateral variations (e.g., upflows and downflows) occurring at scales smaller than or nearly equal to the atmospheric model

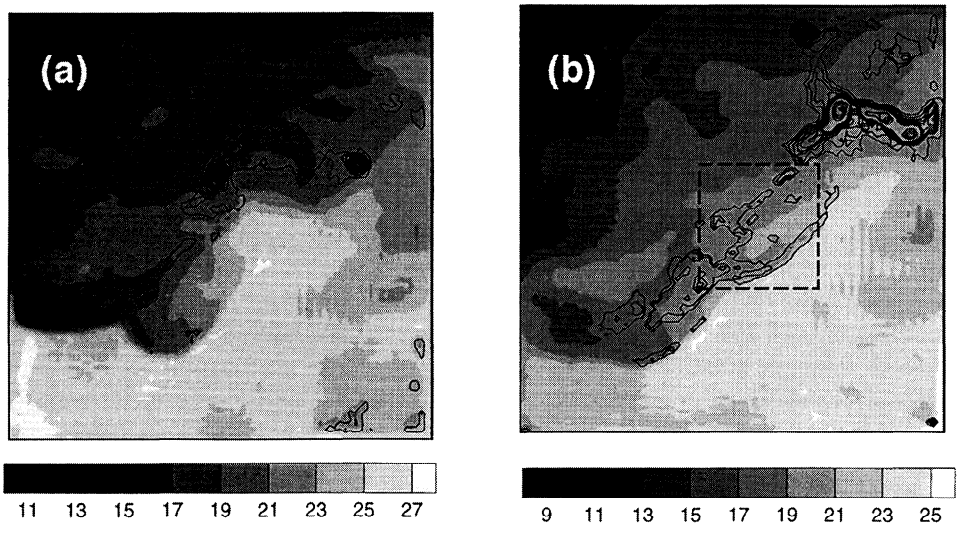

Figure 2. Distribution of ground temperature in degrees Celsius (gray scale map) and rainfall intensity in millimeters per hour (black curves) over the 12 km resolution domain (domain 2 in Figure 1) numerically predicted with run 1 and the physics options listed in columns of domains 1 and 2 in Table 2. Distributions are shown at (a) 15 hours (0300 UTC June 11) and (b) 18 hours (0600 UTC June 11) of simulation time. The peak rainfall intensities are 91.2 mm/h at 15 hours and 81.6 mm/h at 18 hours, which generally correspond to the resolved rainfall and are highly concentrated at a few locations. The dashed frame in Figure 2b marks a zoom-in region in which subgrid-scale rainfall variability is shown in Figure 5.

grid size. Because it is impossible to represent this type of motion with the atmospheric variables determined at the model grids, so-called cumulus parameterization schemes were developed to "represent" the convective motions and their dynamical contribution to the large-scale atmospheric circulations [*Grell*, 1993]. However, these convective parameterization schemes (which are currently available in MM5) were developed for larger-scale models and one should be cautious when using them in higher-resolution simulations. Their use may cause significant problems in total precipitation computation, especially because the so-called "convective" component as computed by MM5 may not accurately represent or capture the actual, physical convective rainfall since the convective parameterization scheme is not always able to model the dynamics of convection at these small scales. This problem renders the total precipitation computation problematic since it is known that the convective rainfall accounts for a substantial part of the total precipitation and that its feedback to larger-scale dynamical processes is important [*Liu et al.*, 1996; *Zhang et al.*, 1989; *Grell*, 1993]. It is noted that throughout this paper, unless specified otherwise, the term "convective rainfall" component is used in consistency with the MM5 terminology.

Figure 2 shows the distribution of ground temperature and total (convective plus resolved) rainfall in the 12 km resolution domain (marked by the inner solid frame in Figure 1) computed with run 1 at 15 hours (Figure 2a) and 18 hours (Figure 2b) of simulation time. The simulated rainfall appears at the appropriate time and location following the development of the squall line, as verified visually against the observations (see *Zhang et al.* [1989] for surface analysis and radar images of this squall line storm). Because the objective of this study is to develop a hybrid approach and examine its usefulness for predicting rainfall over a large range of scales, here we will not present a description of the meteorological features of this storm system, instead focusing our attention only on the rainfall and $CAPE$ variations. Interested readers can find a detailed and thorough examination of the dynamical features associated with this intense squall line development in the work by *Zhang et al.* [1989], who used a hydrostatic atmospheric model (MM4) with 24 km resolution. The simulated results in our study are quite similar to theirs.

3.2. Selection of a Representative $CAPE$

It is noted that the premise of the developed hybrid approach is based on the assumption that a representative $CAPE$ can be found, which is sensitive to the changes of the meteorological conditions during the storm evolution. If such a $CAPE$ can be found and used in (3) and (4) to predict the subgrid-scale rainfall variability, the hybrid approach would realize its advantages over other current approaches. For addressing the question of whether a representative $CAPE$ can be found, it is necessary to examine the spatial distribution of $CAPE$ and its relationship to the development of the squall line and the associated rainfall patterns.

Figure 3 shows the spatial distribution of $CAPE$ in domain 2 at different simulation times from run 1. The spatial variation of $CAPE$ is characterized by a large-area low-gradient (< 100 m^{2}s^{-2}) and a few localized high-gradient zones (> 2000 m^{2}s^{-2}), which generally coincide with the convergence locations of wind velocity near the ground. One should note that the logarithmic transform of $CAPE$ (as shown in Figure 3) illustrates better the correlation of its high-energy zones with the propagation of the squall line. In this simulation as verified against observation, the squall line appears after 0000 UTC June 11 (12 hours of simulation time). Interestingly, the high $CAPE$ zone at this instance has shown a direction change toward SW-NE (Figure 3b). Then, the high $CAPE$ zone moves southeasterly together with the squall line. By 0600 UTC June 11 (18 hours of simulation time) the high $CAPE$ zone has migrated to the southeastern corner of the studied region (Figure 3d) while in the area of inactivity $CAPE$ is very small. The rainfall indicated by the white curves in Figure 3 occurs outside, but close to the high $CAPE$ zones (Figure 3a). After the squall line appears (12 hours of simulation time), the rainfall belts closely follow after the high $CAPE$ zones (Figures 3c and 3d). Such an association of $CAPE$'s spatial pattern change with the squall line development clearly demonstrates that $CAPE$ is a sensitive variable to the meteorological conditions of the storm environment.

The fact that high $CAPE$ concentrates at a few locations in front of the squall line at a given time facilitates the choice of a representative $< CAPE >$ using (8). The low $CAPE$ values, i.e., the values smaller than a selected cutoff value K_s, can be filtered out since this part of the convective energy shows little spatial correlation with the moving of the squall line. Figure 4 shows the temporal variations of $< CAPE >$ defined by (8) for selected values of K_s equal to 800 m^{2}s^{-2} (the dashed curve), 1000 m^{2}s^{-2} (the solid curve) and 1200 m^{2}s^{-2} (the dot-dashed curve), respectively. One interesting observation is that the undulations of $< CAPE >$ with simulation time are not sensitive to the actual values of K_s, confirming the representativeness of the determined $< CAPE >$. Two lows of $< CAPE >$ appear at 2 hours and 13 hours of the simulation time in all three curves. Moreover, the undulation of $< CAPE >$ indicates the possibility of its dynamical updating, which is a particular advantage of the proposed downscaling scheme. The first low of $< CAPE >$ is due to the initial adjustment of the dynamical process to the imposed initial and boundary conditions, which do not satisfy the conservation laws. Examination of the relationship between the $< CAPE >$ variation and the squall line evolution demonstrates that the second low of $< CAPE >$ is closely related to the first appearance of the squall line, which causes the convective energy change. Therefore, we believe that the $< CAPE >$

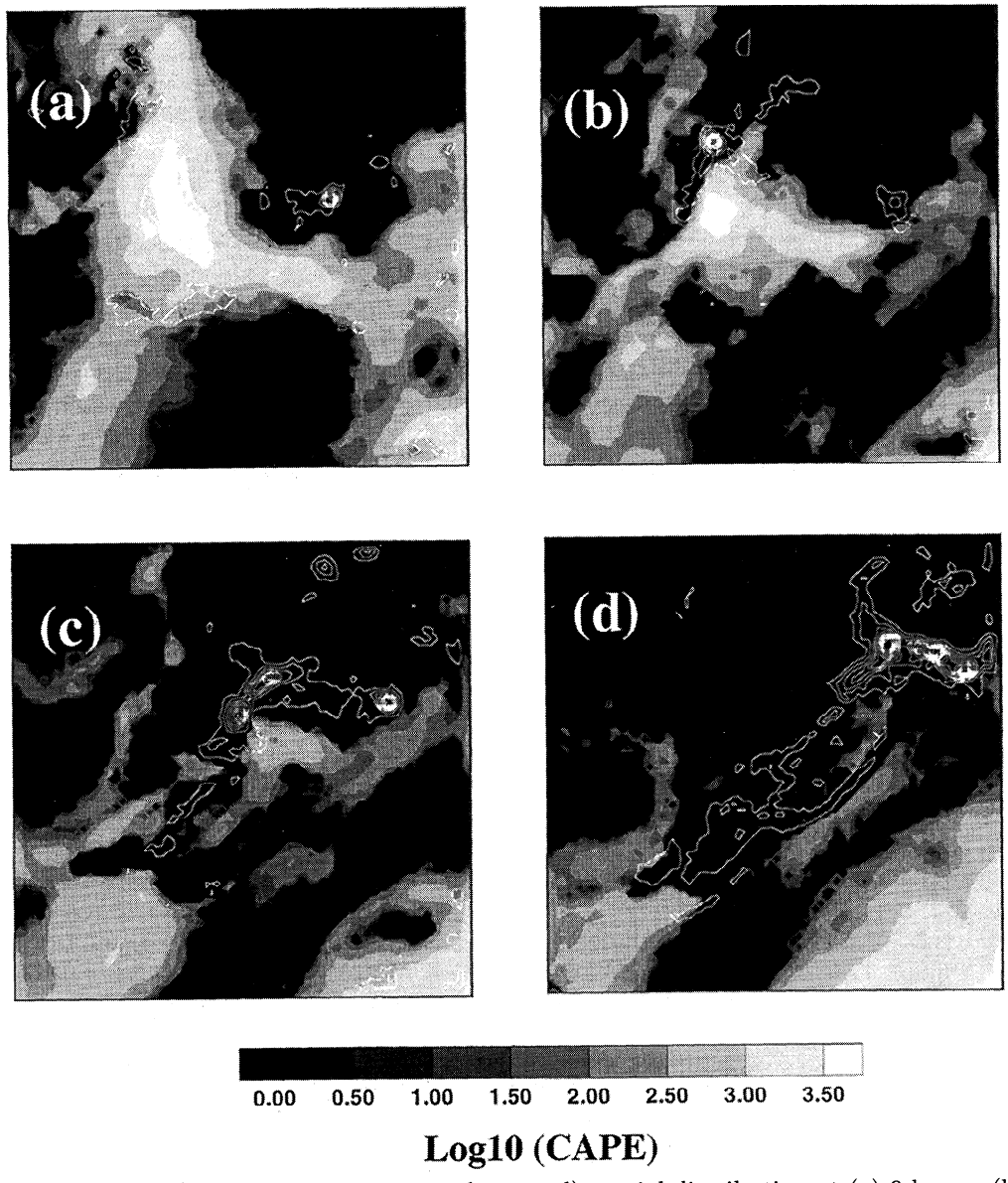

Figure 3. *CAPE* (square meters per second squared) spatial distribution at (a) 9 hours, (b) 12 hours, (c) 15 hours, and (d) 18 hours of simulation time, in the same run (run 1) as in Figure 2. The gray scale variation is shown for the logarithmic transform of *CAPE*. The white curves indicate the rainfall distribution.

given by (8), although quite simple, is dynamically informative and can be used for linking the dynamical computation of rainfall with its subgrid-scale variability prediction.

The small solid squares in Figure 4 (connected with a dotted curve) are the *CAPE* values determined from observed sounding data at stations in Kansas and Oklahoma [*Perica and Foufoula-Georgiou*, 1996a]. Referring to this dotted curve, we select $K_s = 1000$ m^{2}s^{-2} for determining the representative $< CAPE >$ for this storm because this yields a better fit (the solid curve) to the real *CAPE* than the other curves corresponding to other values of K_s. The K_s value of 1000 m^{2}s^{-2} is kept unchanged over the storm evolution so that a meaningful comparison of the changes in the convective energy as the storm evolves can be made using the values of representative $< CAPE >$.

In the control run (run 1), the total rainfall before 0000 UTC June 11 (or 12 hours of simulation) is mainly contributed by the parameterized components (i.e., convective rainfall). After that, resolved rainfall appears with high intensity, but highly concentrated at a few locations. In contrast, the convective component of rain is widely distributed following the squall line propagation. The ratio of the peak value of convective rainfall to the resolved rainfall becomes 30-40% by 0600 UTC June 11, indicating that the convective strength has been reduced after the resolved rainfall is produced. On the other hand, the computed values of $< CAPE >$ shown in Figure 4 after 0040 UTC June 11 (16 hours of

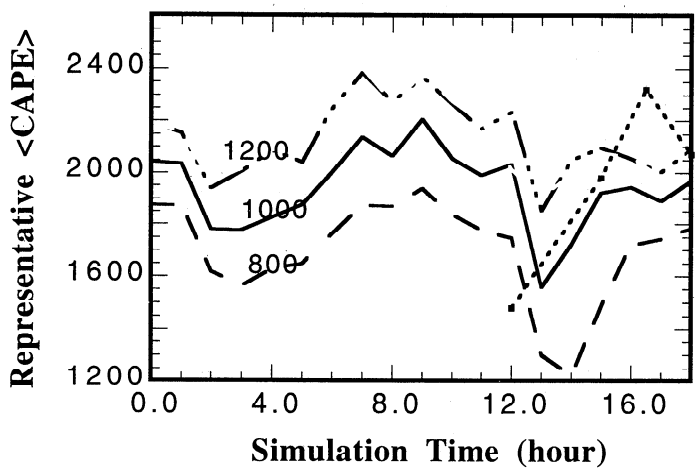

Figure 4. Temporal variations of representative CAPE determined using (8) for selected value of K_s equal to 800 m^2s^{-2} (the dashed curve), 1000 m^2s^{-2} (the solid curve) and 1200 m^2s^{-2} (the dot-dashed curve), respectively, obtained from the spatial variations of $CAPE$ shown in Figure 3. The small solid squares connected with the dotted curve are the $CAPE$ values determined using (5) for the sounding data observed at stations in Kansas and Oklahoma.

simulation time) show a decreasing trend different from the real case. These results indicate that the convective strength and its duration in this control run are slightly lower than the convective energy required for the natural squall line development, although very similar dynamical features have been reproduced by this simulation.

3.3. Effect of Subgrid-Scale Rainfall Variability

Next, we will activate the SDS and FERSV modules while keeping the input parameters same as in run 1 and see whether the feedback effects of subgrid-scale rainfall variability can improve the convection persistence and the short-term rainfall predictions. The subgrid regime in Table 1 is made over domain 2 with subgrid lengths dyadically smaller. That is, starting from the 12 km grids, we downscale rainfall to resolutions of 6 km, 3 km and 1.5 km. For a better illustration of the details, Figure 5 shows the images of the subgrid-scale rainfall redistribution in a small zoom-in area (marked by the dashed frame in Figure 2b) of domain 2 at resolutions of 6.0 km, 3.0 km and 1.5 km, respectively, downscaled by the SDS from the 12 km resolution rainfall field, which is computed with run 1 over domain 2. The most striking observation is that the local rainfall intensity increases dramatically as the resolution increases in the subgrid regime while keeping the total rain mass conserved. Such a large change of the local rainfall intensity in the subgrid regime will certainly have some impact on the local ground energy budget and water partitioning, which in turn will affect the dynamical processes in the atmosphere.

In order to describe the feedback effects of the subgrid-scale rainfall spatial variability, we have quantitatively compared the rainfall and other dynamical features between the runs with (run 2) and without (run 1) including the feedback effects. Significant changes are found in the local distribution of rainfall and some related physical variables (e.g., ground temperature) whereas the overall squall line pattern is not very sensitive to the rainfall redistribution. Before the resolved rainfall appears, the feedback effects are very small. However, once the resolved rainfall occurs, the effects start to accelerate. By 0600 UTC June 11 (18 hours of simulation time), the positive and negative changes in rainfall due to the feedback effects (shown in Figure 6 by the black and white curves, respectively) are comparable in magnitude to the rainfall computed without considering the feedback effects (shown in Figure 2b). Ground temperature changes of up to 5°C are observed. Relatively strong reduction of the ground temperature takes place just ahead of the squall line center.

Comparison of the rainfall changes in Figure 6 with the rainfall intensities in Figure 2b shows the interesting finding that the negative peak change of rainfall in Figure 6 is located just at the place where resolved rainfall heavily occurs in Figure 2b (upper right area). The high-intensity rainfall increases the local moisture availability, which further causes a redistribution of water content in the cloud. As a positive feedback effect, the resolved rainfall pattern and intensity show clear changes. In contrast, the convective rainfall changes are not so dramatic for two reasons: (1) Although convective rainfall covers a large area, the intensities are much lower than the resolved rainfall. The local moisture availability increases are, hence, minor in the area where the convective rainfall occurs. Consequently, the feedback effects on the convective rainfall are relatively weak. (2) No explicit shallow convection parameterization is included in the simulation because such a scheme is not available yet. However, as demonstrated by *Avissar and Liu* [1996], the shallow convection processes are

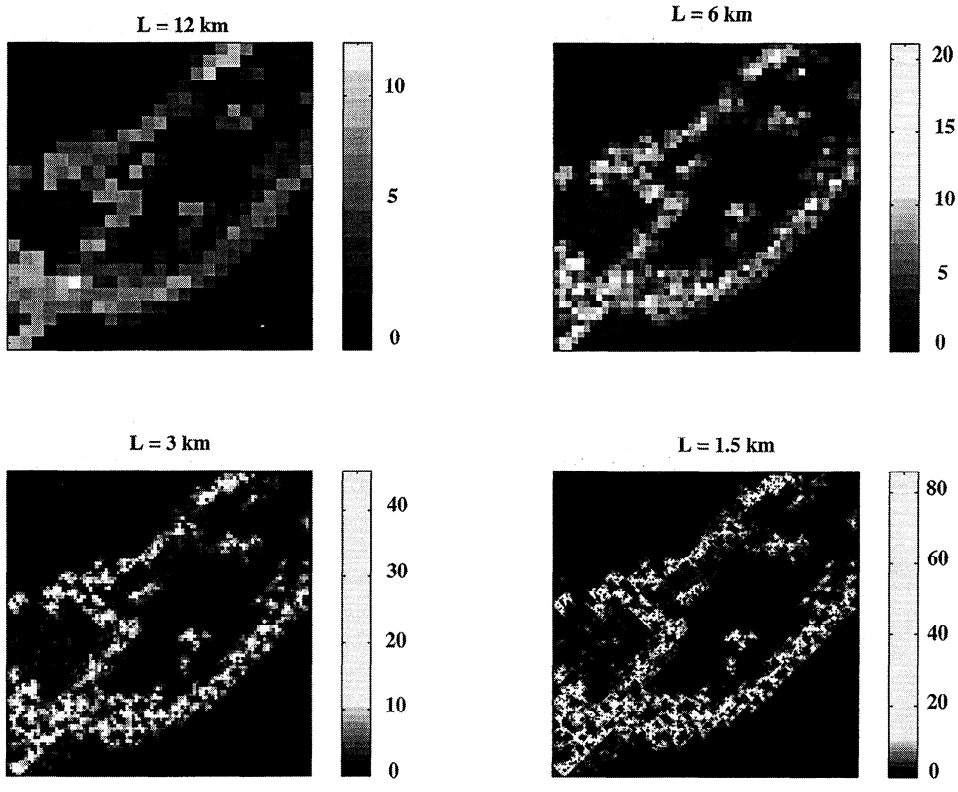

Figure 5. Rainfall redistribution in millimeters per hour predicted with the statistical downscaling scheme over the subgrid regime with resolution of 6.0 km, 3.0 km, and 1.5 km, respectively. The $L = 12$ km image is the rainfall distribution over the zoom-in area marked with the dashed frame in Figure 2b computed with run 1. Note that in order to better illustrate the increase of the local rainfall intensities as scale decreases, we have kept the gray scale map the same in all panels (such that pixel intensities greater than 11 mm/h are displayed as nearly white color). However, we have shown the range of actual rainfall intensities at each scale to demonstrate that they change dramatically as scale decreases.

very important for evaluating the feedback effects of the subgrid-scale rainfall variability and can dramatically change the convective rainfall generation efficiency.

The solid and dashed curves in Figure 7 show the temporal variations of $< CAPE >$ for run 1 and run 2, respectively. The difference of these two curves arises from the feedback effect of subgrid-scale rainfall variability. Basically, this effect on the $< CAPE >$ is small, except at 12 hours of simulation when the resolved rainfall occurs with high intensity. This result is not unexpected because the feedback effect is mainly associated with the resolved rainfall, which is highly concentrated in a small area. Unfortunately, inclusion of the subgrid-scale rainfall variability does not improve the fit of the predicted convection persistence after 16 hours of simulation to the observed $CAPE$ (the dotted curve in Figure 4).

The dash-dotted curve in Figure 7 is obtained with run 3 using the physics options listed in the domain 1 column of Table 2 and turning off domains 2 and 3. The difference between the solid curve and the dash-dotted curve in Figure 7 shows the effects of decreasing the atmospheric model resolution. Big differences in the $< CAPE >$ values between the two runs appear after 12 hours of simulation time. In the 12 km resolution simulation (run 1), a $< CAPE >$ low occurs at 13 hours whereas it appears at 16 hours in the simulation of 36 km resolution (run 3).

Figure 8 shows the $CAPE$ spatial variations during the evolution of the squall line structure in the same area as in Figure 3, but from the 36 km resolution simulation of run 3. In the low-resolution regime, the spatial variation of $CAPE$ does not show clear orientation until the 16 hours of simulation when the squall line appears and causes the second low of the representative value of $< CAPE >$ shown with the dash-dotted curve in Figure 7. Comparison of the storm features between run 3 and run 1 also shows that the location of the squall line in the former case is 3 hours after that in the latter case along the propagation direction of the squall line. Inclusion of the subgrid-scale rainfall variability in run 3 does not improve the delay of occurrence time of the squall line. These results imply that if the 36 km resolution is used in the atmospheric simulation, some important dynamics of the storm are not well captured, at least with the selected physics options (the domain 2

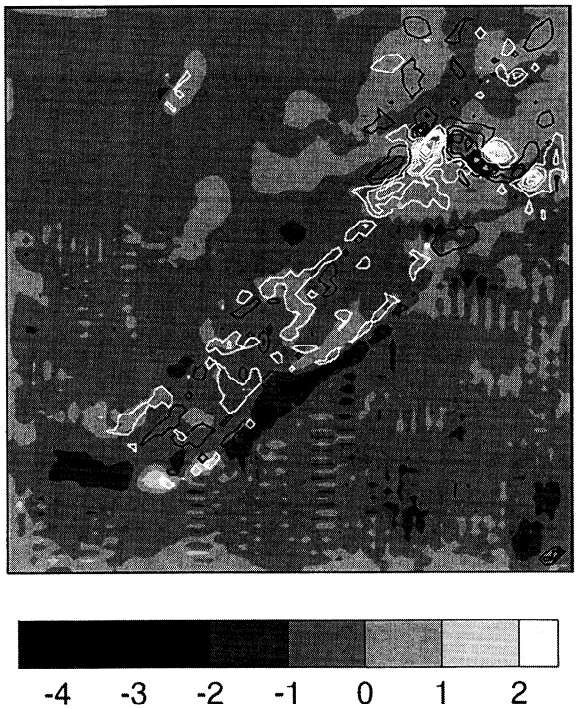

Figure 6. Changes of ground temperature in degrees Celsius (gray scale variation) and rainfall intensity in millimeters per hour (black and white curves) caused by adding the feedback effect of subgrid-scale rainfall variability to the simulation of run 1. The temperature (or rainfall) change is measured by the difference between the temperature (or rainfall) field computed with run 2 and run 1 at 18 hours of simulation time. The black and white curves indicate the increase and decrease of rainfall intensity with peak values of 55.2 mm/h and 66.6 mm/h, respectively.

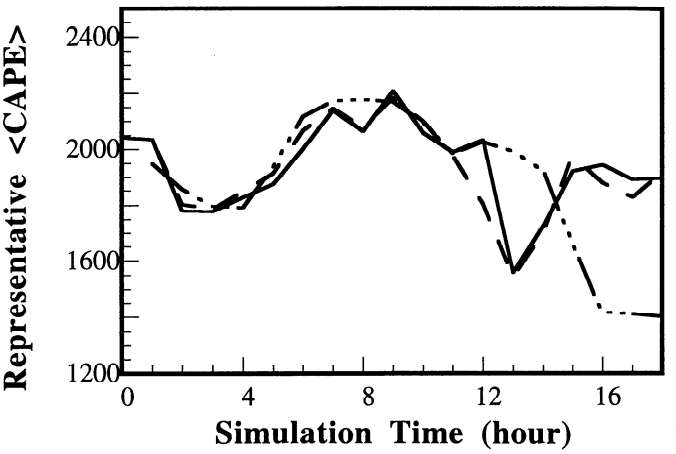

Figure 7. Temporal variations of representative CAPE in square meters per second squared from three runs. The solid, dashed, dash-dotted curves are respectively from runs 1, 2, and 3 in Table 1. The difference between the solid and dashed curve indicates the feedback effect of subgrid-scale rainfall variability, and the difference between the solid and dash-dotted curve indicates the effect of increasing the MM5 model resolution.

column of Table 2), and inclusion of the feedback effect of subgrid-scale rainfall redistribution cannot make up for these lost atmospheric dynamics. In contrast, the parameterized cloud and precipitation dynamics work more effectively when the 12 km resolution domain is nested in run 1 and make the predictions of storm dynamical features and rainfall patterns more successful (Figure 2), as compared against observations.

3.4. Comparison of High-Resolution MM5 Results With the Hybrid Model Results

With the rapid increase of computer power, high-resolution computation of dynamical processes in the atmosphere becomes feasible. By using the multinesting capability of the MM5, one can compute rainfall variability at resolution of a few kilometers. Thus, it would be interesting to investigate whether a continued increase of the atmospheric model resolution can improve the fit of the model predictions to the observations and to determine the difference between rainfall variability predicted by the hybrid approach and the rainfall computed purely by the MM5 model with high resolution. For addressing these questions, we have performed another numerical experiment using three-level nesting, which is run 4 in Table 1. In this run, all the three domains shown in Figure 1 are used and nested two-way interactively. The physics options used for each domain are listed in Table 2. In this run, the convective cumulus parameterization is not used in the 4 km resolution area (domain 3) because the dynamical processes of convective cumulus in the high-resolution regime may not be described very well by the parameterization schemes developed for large-scale models [*Liu and Avissar*, 1996; *Kuo et al.*, 1996; *Colle and Mass*, 1996]. The simulation results are somehow not encouraging. The squall line was not simulated well at all (see the distribution of the ground temperature in Figure 9). The rain (the white

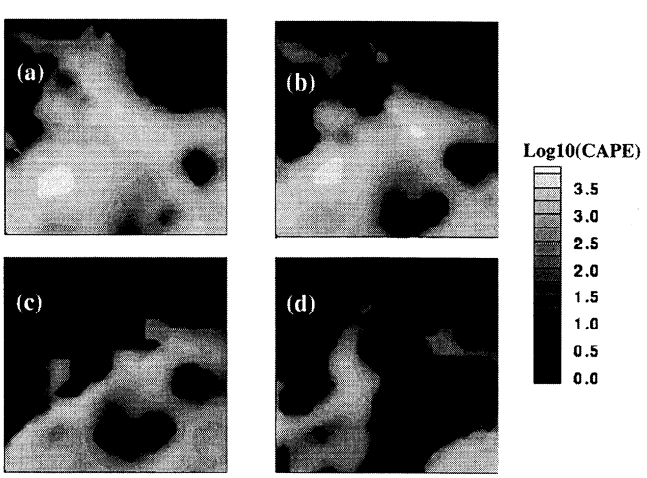

Figure 8. *CAPE* (square meters per second squared) spatial distribution at (a) 12 hours , (b) 14 hours, (c) 16 hours, and (d) 18 hours of simulation time from run 3.

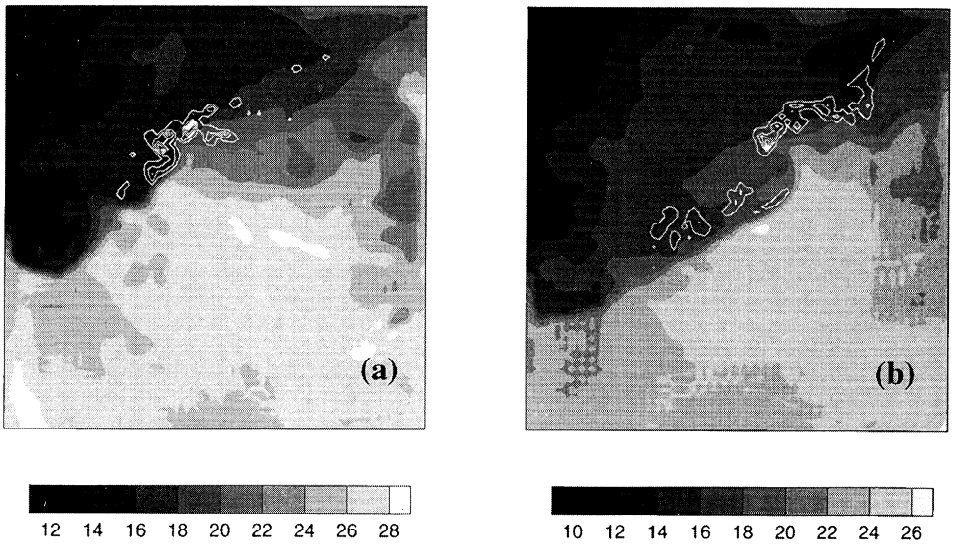

Figure 9. Rainfall intensity in millimeters per hour (the white curves) and temperature in degrees Celsius (gray scale variation) distributions computed with run 4 at (a) 15 hours and (b) 18 hours of simulation time. The peak values of rainfall intensity are 34.8 mm/h in Figure 9a and 31.2 mm/h in Figure 9b.

curves in Figure 9) occurs only at a few small areas and does not show the correct orientation as in run 1 (Figure 2), indicating that further increase of the MM5 grid resolution degrades the quality of the simulation. In addition, the computational cost of run 4 is 45 times larger than that of run 1, and 40 times larger than that of run 2. Note that run 2 includes the computations of subgrid-scale rainfall variability and its feedback effects, which increase the cost of the atmospheric model run by less than 15%.

The reason for the degraded quality in rainfall prediction with increased resolution in run 4 is probably due to the fact that no convective cumulus parameterization was used in the 4 km resolution regime and thus no convective rainfall component could be generated. Recall that we have used the conventional initial and boundary conditions for starting the simulation, and because of the "spin-up" problem [*Wu et al.*, 1995], which often exists in this type of atmospheric dynamical simulation, no resolved rainfall is generated before 12 hours of simulation [*Zhang et al.*, 1989; *Grell*, 1993]. In this case, convective parameterization is necessary for the explicit moisture scheme to become active and produce rainfall in the 4 km resolution mesh because the explicit scheme can be activated only if the air becomes saturated. In addition, *Zhang et al.* [1989] and *Grell* [1993] have shown that the existence of downdrafts parameterized through the convective cumulus scheme plays a decisive role in whether the June 10-11, 1985 storm with an intense squall line can be simulated successfully. However, at this time there is no good scheme available for parameterizing the convective cumulus in a model of resolution of a few kilometers. Turning-on the cumulus parameterization available in the MM5 code in the 4 km mesh is also problematic because these cumulus schemes were developed for larger-scale cloud and precipitation processes and may not be appropriate for the high-resolution simulation [*Liu and Avissar*, 1996]. The recent work by Avissar's group has shown that at the grid scale of a few kilometers, the cloud microphysical processes still need to be parameterized [*Liu and Avissar*, 1996] and the spatial distribution of clouds and precipitation is quite sensitive to the cloud microphysical processes [*Avissar and Liu*, 1996]. Overall, it is certainly difficult to physically parameterize the dynamical process of clouds and precipitation at small scales of a few kilometers [*Kuo et al.*, 1996], and this is an issue that needs further investigation.

4. Conclusions

The study reported in this paper has two important aspects in its scientific contribution. The first one is the development of a dynamical/statistical hybrid approach, which provides a useful and cost-effective scheme to predict rainfall at subgrid scales (around 1 km) based on larger-scale atmospheric model predictions. A key parameter of the proposed scheme is $CAPE$ (convective available potential energy), which links the statistical downscaling description with the large-scale dynamical computation of rainfall. A representative value of $CAPE$, which is sensitive to changes of the meteorological conditions during the storm evolution, has been introduced based on the examination of the spatial and temporal variations of $CAPE$ during the storm of June 10-11, 1985 of the PRESTORM field experiment. Good correlation has been found between the high $CAPE$ zones and the propagation of the squall line. Accordingly, the defined representative value $< CAPE >$ is sensitive to the changes of dynam-

ical conditions of the storm environment. Therefore, the hybrid approach developed in this study offers the advantage, in contrast to other currently used downscaling schemes, of providing the dynamical information needed for statistically predicting the subgrid-scale rainfall variability based on dynamically updating the value of $< CAPE >$ as the storm evolves.

One important observation is that the redistributed rainfall exhibits much higher local intensities compared to those predicted by the MM5 model. Such higher intensities are expected to have an important effect on the surface energy and water partitioning [*Brubaker and Entekhabi*, 1996; *Faures et al.*, 1995]. They also indicate the importance of "scale" in atmospheric model validation; i.e., the atmospheric model rainfall output, which represents the average over a grid box of particular size, is certainly not directly comparable to the rainfall intensity measured at any single rain gauge within the model grid box. Rather, scaling relationships as those found by us or by other authors [e.g., *Gupta and Waymire*, 1993; *Tessier et al.*, 1993] could be used to link local rainfall intensities to average intensities predicted by atmospheric models over larger grid boxes.

The other accomplishment of this work is the investigation of the feedback effects from the subgrid-scale rainfall spatial variability on the further development of rainfall in atmospheric models. The simulated results for the June 10-11, 1985 squall line indicate that the feedback effects are significant in affecting the rainfall development in the 24 hour simulation. A similar finding was reported by *Diak et al.* [1986] when the variations of moisture availability were considered. The effect of subgrid-scale variabilities, especially of rainfall, is expected to become stronger if appropriate parameterization of the small-scale cloud and precipitation microphysics is included [*Liu and Avissar*, 1996; *Avissar and Liu*, 1996]. *Mölders and Raabe* [1996] also reported that the feedback effects of surface heterogeneities on cloud and precipitation processes in 5 km resolution simulations are much stronger than those in 10 km resolution simulations.

One should note that the feedback effects in this study are considered by changing the moisture availability in the subgrid regime according to the local rainfall intensity. Although this assumption is sound, determination of the ground temperature, heat and moisture fluxes has been done in a simplified manner (same as the high-resolution Blackadar planetary boundary layer model). More realistic parameterization of the ground energy and water balances in the subgrid regime [e.g., *Xue et al.*, 1991; *Dickinson et al.*, 1994; *Sivapalan and Woods*, 1995] needs to be incorporated and more cases need to be studied in the future in order to better understand the feedback effects of the subgrid-scale rainfall variability and its role in improving atmospheric and surface variable predictions.

It is noted that a recent work by *Wang and Seaman* [1997], which appeared after our paper was accepted for publication, reports findings on the resolution dependence of the June 10-11 squall line simulation using MM5, which agree with our findings. The reader is encouraged to consult this paper for a comprehensive comparison of several convective parameterization schemes and the effects of resolution (grid size) on the simulation results.

Appendix: Dependence of M, Z_L and C_{ap} on Subgrid-Scale Rainfall Intensity

Moisture availability M is a dimensionless parameter, whose value varies between 0 and 1 corresponding to wetness change from complete dry to complete wet. The dependence of M on rainfall is specified on the basis of slab thickness [*Grell et al.*, 1994]. According to the MM5 code, the slab thickness in the boundary layer is less than 10 cm, and 25 mm of rainfall accumulated in 1 hour is considered enough to completely saturate an initially dry ($M = 0$) slab. The moisture availability at any subgrid point i M_i is assumed to vary with the subgrid-scale rainfall intensity f_i (millimeters per hour) according to the following formula:

$$M_i = \begin{cases} M_0 & \text{if } f_i < 5 \\ M_0 + (1 - M_0)\frac{f_i - 5}{20} & \text{if } 5 \le f_i \le 25 \\ 1.0 & \text{if } f_i > 25 \end{cases} \quad \text{(A1)}$$

Soil roughness $Z_{L,i}$ is quite sensitive to the local water content and variations of moisture availability [*Diak et al.*, 1986]. Hence, we adjusted the roughness $Z_{L,i}$ according to M_i:

$$Z_{L,i} = \begin{cases} Z_{L0} & \text{if } M_i < 0.85 \\ 0.01 & \text{if } M_i \ge 0.85 \end{cases} \quad \text{(A2)}$$

Table 3. Parameters Used in (A1) to (A3)

Parameter	Definition	Units
M_0	reference moisture variability	dimensionless
Z_{Lo}	reference roughness	cm
K	soil heat capacity	$\mathrm{Jm^{-3}K^{-1}}$
c	water heat capacity	$\mathrm{Jm^{-3}K^{-1}}$
Ω	the Earth's angular velocity	
λ_j	empirical constants, $j = 1, 2, 3, 4$	
N	number of grid boxes surrounding one MM5 grid	

Values of these parameters at the subgrid regime are kept the same as at the corresponding MM5 grid.

In (A1), the soil moisture availability at the ith point is set to the reference value M_0 if f_i is smaller than a threshold value of 5 mm/h to maintain numerical stability in computing the ground temperature, moisture and heat fluxes at the subgrid points, over which rainfall intensity changes dramatically from one grid to another. For the same reason, a threshold value of 0.85 is used for M_i in (A2) for specifying the subgrid-scale variation of the soil roughness $Z_{L,i}$.

The same expression (equation (A3)) as in the MM5 code is used for evaluating the thermal capacity C_{ap} ($\mathrm{Jm^{-3}K^{-1}}$), but replacing the moisture availability at the MM5 model grid with the mean value at the subgrids encompassing this particular model grid,

$$C_{ap} = 0.95\sqrt{\frac{C_\Sigma \Psi_\Sigma}{2\Omega}} \tag{A3}$$

where

$$C_\Sigma = K + \frac{0.25c}{N}\sum_{i=1,}^{N} M_i$$

$$\Psi_\Sigma = \frac{1}{N}\sum_{i=1}^{N}(\lambda_4 + \lambda_3 G_{1i} + \lambda_2 G_{2i} + \lambda_1 G_{3i})$$

$$G_{1i} = 250M_i, G_{2i} = G_{1i}^2, G_{3i} = G_{1i}^3$$

Table 3 lists all the constants and other parameters used in (A1) to (A3).

Acknowledgments. We benefited from discussions with Brian Colle, Yongqian Liu and Yong Zheng. Shuxia Zhang wants to thank Sanja Perica for providing the Matlab program of implementing the statistical downscaling scheme and A. Carsteanu and V. Venugopal for their help in formating this paper. This research was supported by NOAA's Office of Global Programs under grant NA46GP0486. We thank the Minnesota Supercomputer Institute and the National Center for Atmospheric Research for their generous support of computing resources.

References

Air Weather Service, The use of skew T, log P diagram in analysis and forecasting, Report, Scott Air Force Base, Ill., 1979.

Avissar, R., and Y.-Q. Liu, Three-dimensional numerical study of shallow convective clouds and precipitation induced by land surface forcing, *J. Geophys. Res.*, **101**(D3), 7499-7518, 1996.

Brubaker, K.L., and D. Entekhabi, Analysis of feedback mechanisms in land-atmosphere interaction, *Water Resour. Res.*, **32**(5), 1343-1357, 1996.

Colle, B.A. and C.F. Mass, An observational and modeling study of the interaction of low-level southwesterly flow with the Olympic Mountains during COAST IOP 4, *Mon. Weather Rev.*, **124**, 2152-2175, 1996.

Cunning, J.B., The Oklahoma-Kansas Preliminary Regional Experiment for STORM-Central, *Bull. Am. Meteorol. Soc.*, **67**(12), 1478-1486, 1986.

Diak, G., S. Heikkinen, and J. Bates, The influence in surface treatment on 24-hour forecasts with a limited area model, including a comparison of modeled and satellite-measured surface temperatures, *Mon. Weather Rev.*, **114**, 215-232, 1986.

Dickinson, R. E., A. Henderson-Sellers, P.J. Kennedy, and F. Giorgi, Biosphere-Atmosphere Transfer Scheme (BATS) Version 1e as coupled to the NCAR Community Climate Model, *NCAR Tech. Note*, 1992.

Fan, Y., E.E. Wood, M.L. Baeck, and J.A. Smith, Fractional coverage of rainfall over a grid: Analysis of NEXRAD data over the southern plains, *Water Resour. Res.*, **32**(9), 2787-2802, 1996.

Faures, J.M., D. C. Goodrich, D. A. Woolhiser, and S. Sorooshian, Impact of small-scale spatial rainfall variability on runoff modeling, *J. Hydrol.*, **173**, 309-326, 1995.

Grell, G.A., Prognostic evaluation of assumptions used by cumulus parameterization, *Mon. Weather Rev.*, **121**, 764-787, 1993.

Grell, G.A, J. Dudhia, and D.R. Stauffer, A description of the 5th-generation Penn State/NCAR mesoscale model (MM5), *NCAR Tech. Note NCAR/TN-398 +STR*, 1994.

Gupta, V.K., and E. Waymire, A statistical analysis of mesoscale rainfall as a random cascade, *J. Appl. Meteorol.*, **32**(2), 251-267, 1993.

Kumar, P. and E. Foufoula-Georgiou, A multicomponent decomposition of spatial rainfall fields, 1. Segregation of large and small scale features using wavelet transforms, *Water Resour. Res.*, **29**(8), 2515-2532, 1993a.

Kumar, P. and E. Foufoula-Georgiou, A multicomponent decomposition of spatial rainfall fields, 2. Self-similarity in fluctuations, *Water Resour. Res.*, **29**(8), 2533-2544, 1993b.

Kumar, P., and E. Foufoula-Georgiou, Characterizing multiscale variability of zero intermittency in spatial rainfall, *J. Appl. Meteorol.*, **33**(12), 1516-1526, 1994.

Kuo, Y.-H., J. Bresch, M.-D. Cheng, J. Kain, D.B. Parson, W.-K Tao, and D.-L. Zhang, Summary of a mini-workshop on cumulus parameterization for mesoscale models, *NCAR Tech. Note*, 1996.

Liu, Y.-Q., and R. Avissar, Sensitivity of shallow convection precipitation induced by land surface heterogeneities to dynamical and cloud microphysical parameters, *J. Geophys. Res.*, **101**(D3), 7477-7497, 1996.

Liu, Y.-Q., R. Avissar and F. Giorgi, Simulation with the regional climate model RegCM2 of extremely anomalous precipitation during the 1991 east Asian flood: An evaluation study, *J. Geophys. Res.*, **101**(D21), 26,199-26,215, 1996.

Lorenz, E. N., Atmospheric predictability as revealed by naturally occurring analogues, *J. Atmos. Sci.*, **26**, 636-646, 1969.

Mölders, N., and A. Raabe, Numerical investigations on the influence of subgrid-scale surface heterogeneity on evapotranspiration and cloud processes, *J. Appl. Meteorol.*, **35**, 782-795, 1996.

Perica, S., and E. Foufoula-Georgiou, Linkage of scaling and thermodynamic parameters of rainfall: Results from midlatitude mesoscale convective systems, *J. Geophys. Res.*, **101**(D3), 7431-7448, 1996a.

Perica, S., and E. Foufoula-Georgiou, A model for multiscale disaggregation of spatial rainfall based on coupling meteorological and scaling descriptions, *J. Geophys. Res.*, **101**(D21), 26,347-26,361, 1996b.

Schaake, J.C., V.I. Koren, Q.-Y. Duan, K. Mitchell, and F. Chen, Simple water balance model for estimating runoff at different spatial and temporal scales, *J. Geophys. Res.*, **101**(D3), 7461-7475, 1996.

Seo, D.-J., and J.A. Smith, Characterization of the climatological variability of mean areal rainfall through fractional coverage, *Water Resour. Res.*, **32**(7), 2087-2095, 1996.

Sivapalan, M., and R.A. Woods, Evaluation of the effects of general circulation model's subgrid variability and patchiness of rainfall and soil moisture on land surface water balance fluxes, in *Scale Issues in Hydrological Modeling*, edited by J.D. Kalma and M. Sivapalan, pp. 453-473, John Wiley, New York, 1995.

Tessier, Y., S. Lovejoy, and D. Schertzer, Universal multifractals in rain and clouds: Theory and observations, *J. Appl. Meteorol.*, **32**, 223-250, 1993.

Thomas, G., and A. Henderson-Sellers, An evaluation of proposed representation of subgrid hydrologic processes in climate models, *J. Clim.*, **4**, 898-910, 1991.

University Corporation for Atmospheric Research, General meteorological package (GEMPAK), version 5.1, reference manual, Unidata Program Cent., Boulder, Colo., 1992.

Vannitsem, S., and C. Nicolis, Predictability experiments on a simplified thermal convection model: The role of spatial scales, *J. Geophys. Res.*, **99**(D5), 10337-10385, 1994.

Vannitsem, S., and C. Nicolis, Dynamics of fine scale variables versus averaged observables in a simplified thermal connection model, *J. Geophys. Res.*, **100**(D8), 16367-16375, 1995.

Wang, W., and N.L. Seaman, A comparison study of convective parameterization schemes in a mesoscale model, *Mon. Weather Rev.*, **125**, 252-278, 1997.

Warrilow, D.A., A.B. Sangster, and A. Slingo, Modeling of land-surface processes and their influence on the European climate, *Dyn. Climatol. Tech. Note* **38**, p. 92, Meteorol. Off., Bracknell, Berkshire, England, 1986.

Wu, X.-H., G. R. Diak, and C. M. Hayden, Short-range precipitation forecasts using assimilation of simulated satellite water vapor profiles and column cloud liquid water amounts, *Mon. Weather Rev.*, **123**, 347-365, 1995.

Xue, Y., P.K. Sellers, J.L. Kinter, and J. Shukla, A simplified biosphere model for global climate studies, *J. Clim.*, **4**, 345-364, 1991.

Zhang, D.-L., K. Gao, and D. B. Parsons, Numerical simulation of an intense squall line during 10-11 June 1985 PRE-STORM, *Mon. Weather Rev.*, **117**, 960-994, 1989.

E. Foufoula-Georgiou and S. Zhang, St. Anthony Falls Laboratory, University of Minnesota, Mississippi River and 3rd Avenue SE, Minneapolis, MN 55414.
(e-mail: efi@mykonos.safhl.umn.edu; sxz@msi.umn.edu)

(Received December 16, 1996; revised March 19, 1997; accepted May 7, 1997.)